

# Analytical spatio-temporal design of Kerr lens mode-locked laser resonators

Kuei-Huei Lin and Wen-Feng Hsieh\*

*Institute of Electro-Optical Engineering, National Chiao-Tung University, Hsinchu, Taiwan*

Received April 17, 1995; revised manuscript received January 2, 1996

An analytical method of spatio-temporal design for a Kerr lens mode-locked Ti:sapphire laser is presented. Various spatial and temporal effects are considered to derive simple quadratic equations of the pulse width for both standing- and traveling-wave cavities. By solving the quadratic equation, we obtain the relations between pulse width and other cavity parameters for a given system for optimal design of a Kerr lens mode-locked cavity and to generate the shortest laser pulses. Our theoretical results agree well with the experimental results, and the computation time of this analytic approach for cavity parameters is reduced drastically as compared with an iteratively numerical approach. © 1996 Optical Society of America.

## 1. INTRODUCTION

After the first realization of Kerr lens mode locking in a Ti:sapphire laser by Spence *et al.*,<sup>1</sup> various theoretical studies were dedicated to the Kerr lens mode-locked (KLM) cavity design both numerically<sup>2</sup> and analytically.<sup>3,4</sup> Among these analytical studies, most efforts were concentrated in the spatial domain by assuming a constant beam-spot size in a thin nonlinear crystal to calculate the nonlinear round-trip loss for different laser powers and cavity designs. Since an optical pulse will undergo self-phase modulation (SPM) as it propagates through a Kerr medium, temporal-domain analysis of a KLM cavity is also important to optimize output pulse width by compensation of the group-velocity dispersion introduced by a laser crystal and SPM. Using a numerical iterative method, Chilla and Martinez<sup>5</sup> adopted a temporal ABCD matrix method<sup>6,7</sup> to discuss the KLM properties of a Ti:sapphire laser. Because their method involves iterative manipulation of a seeding pulse to get steady-state output, a lot of computation time is needed. Also, with the assumption of a constant beam radius in the Kerr medium and without astigmatism compensation, their method has to reduce the nonlinearity by a factor of 3 to meet the experimental result.<sup>8</sup>

In our previous studies,<sup>9,10</sup> by introducing a renormalized  $q$  parameter in a Kerr medium,<sup>11</sup> we obtained a quartic equation of the beam-spot size at the output coupler in a general standing-wave KLM laser cavity and a quadratic equation of that for a ring cavity with astigmatism compensation. Thus the beam-spot variation throughout the Kerr medium can be calculated by ABCD transformation. Based on these spatial results as well as the concept of temporal ABCD transformation,<sup>6,7</sup> we established a general spatio-temporal approach to analyze steady-state KLM cavities. The temporal ABCD matrices included in our formulation to describe various linear and nonlinear temporal effects are nonlinear absorption, near-resonance phase shift, group-velocity dispersion, dispersion compensation, bandwidth limiting, and self-phase modulation. The first two matrices are directly adopted

from Ref. 7, and we derive the other matrices from a coherent pulse transformation integral. Particularly, the spot-size variation in a Kerr medium obtained from the spatial results<sup>9,10</sup> were considered in a SPM matrix.

We further assumed that the peak intensities of intracavity laser pulses are not so high that the commutation of the characteristic matrices of corresponding nonlinear effects still satisfy the commutation law. This is true for a pulse width of not less than 50 fs under intracavity pulse energy of 200 nJ. Therefore we can combine equivalent complex quadratic phase-modulator matrices and nonlinear absorption matrices. By properly choosing a self-consistent point at the cavities for temporal  $p$  parameters, we can derive a simple quadratic equation for pulse width. After solving this quadratic equation, we obtain the relation between pulse width and other cavity parameters. We found that the optimal prism separations are shorter for broader cavity bandwidths, and the pulse width depends more strongly on the prism separation. We also found that the optimal prism separations for high-energy pulses are shorter than for low-energy pulses and that this difference is more distinct in the narrower-bandwidth case. As the intracavity pulse energy increases, the pulse width begins to decrease, which is a result of stronger SPM and generation of more frequency components. Using our formulation, we explain why a traveling-wave cavity is capable of generating shorter pulses than a standing-wave cavity. Since our analytical method has taken into account the beam-radius variation inside the Kerr medium, not only good agreement with experimental results is obtained, but also the computation time is reduced drastically as compared with iteratively numerical methods.<sup>5</sup>

## 2. SPACE-TIME ANALOGY AND TEMPORAL ABCD MATRICES

There exists an interesting analogy between the spatial problem of Fresnel diffraction and the temporal problem of dispersive pulse propagation.<sup>6,7</sup> Under proper change of variables, formulas describing spatial Gaussian beams

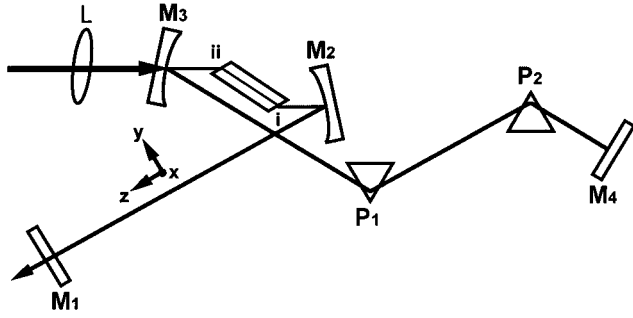


Fig. 1. Four-mirror figure-x standing-wave laser with a Kerr medium of length  $L_c$  placed between two curved mirrors. A pair of Brewster-angle dispersive prisms  $P_1$  and  $P_2$  are placed in the cavity to achieve group-velocity compensation of the laser pulses.

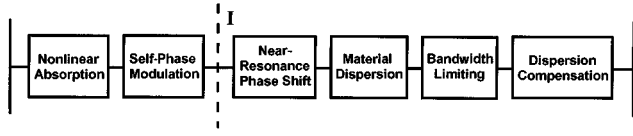


Fig. 2. Block diagram illustrating the six temporal effects in Fig. 1.

can be applied to temporal Gaussian pulses. By this space-time analogy, the exceedingly complicated problem of coherent pulse propagation through a general optical system can be handled in a manner similar to the ray-matrix approach of Gaussian-beam propagation. We may proceed from different starting points to derive the space-time formula analogy. One of the commonly adopted starting points is the analogy between the paraxial wave equation and the dispersive wave equation; another starting point is the analogy between the Fresnel diffraction integral and the coherent pulse transformation integral. These different approaches will lead to different sets of variable substitution in a space-time analogy as well as different temporal matrices. In this paper we adopt the approach of the integral analogy.

By this space-time analogy,<sup>7</sup> we can write the pulse amplitude  $A(\tau)$  and the complex time parameter  $p$  as

$$A(\tau) = A_0 \exp\left(i \frac{c\tau^2}{2p}\right) \exp(ic\tau/\eta), \quad (1)$$

$$\frac{1}{p} = \frac{2\rho}{c} + i \frac{2}{c\sigma^2}, \quad (2)$$

where  $\eta$  is a complex effective refractive index determining the shifts of the central carrier frequency and the position of the pulse maximum and where  $\rho$  and  $\sigma$  are chirping and pulse width of the Gaussian pulse. The temporal ABCD matrix for a dispersive medium of length  $z$  (with refractive index  $n = n_0 + n_1\omega$ ) is

$$M_S = \begin{bmatrix} 1 & S \\ 0 & 1 \end{bmatrix} = \begin{bmatrix} 1 & 2zn_1 \\ 0 & 1 \end{bmatrix}; \quad (3)$$

where  $S = 2n_1z$ , and the matrix for phase modulator [with transmission coefficient  $T = T_0 \exp(iat^2 + ibt)$ ] is

$$M_a = \begin{bmatrix} 1 & 0 \\ \frac{2a}{c} & 1 \end{bmatrix}. \quad (4)$$

The  $p$  parameter is equivalent to the spatial  $q$  parameter and satisfies the temporal ABCD law as

$$p_{\text{out}} = \frac{A_t p + B_t}{C_t p + D_t}, \quad (5)$$

where  $A_t$ ,  $B_t$ ,  $C_t$ , and  $D_t$  are the temporal matrix elements.

For the four-mirror figure-x standing-wave Ti:sapphire laser with intracavity dispersion-compensation prisms shown in Fig. 1, the equivalent block diagram considering various linear and nonlinear temporal effects are shown in Fig. 2, including material dispersion of the crystal, group-velocity dispersion compensation, bandwidth limiting, near-resonance phase shift, nonlinear absorption, and self-phase modulation. The above effects also exist in the four-mirror figure-8 traveling-wave cavity of Fig. 3, and the equivalent block diagram is shown in Fig. 4. In our formulation we do not consider the interplay between SPM and dispersion in the Kerr medium; i.e., we assumed that the peak intensities of intracavity laser pulses are not so high such that the commutation of these characteristic matrices of corresponding nonlinear effects still holds. This approximation can give reasonable agreements with experimental results for a pulse duration longer than 50 fs. For KLM cavities capable of generating shorter pulses, numerical methods must be adopted to obtain better predictions.

The near-resonance phase shift and nonlinear absorption matrices can be found in Ref. 7. For a near-resonance phase shift,

$$M_{NR} = \begin{bmatrix} 1 & -iN\sigma_c z T_2^2 c \\ 0 & 1 \end{bmatrix} = \begin{bmatrix} 1 & -iGT_2^2 c \\ 0 & 1 \end{bmatrix}, \quad (6)$$

where  $N$  is the population inversion,  $\sigma_c$  is the cross section,  $T_2$  is the transverse relaxation time of the transition, and  $G$  is the single-pass power gain. For nonlinear absorption with transmission coefficient  $T = T_0 \exp[\kappa|A(\tau)|^2]$ ,

$$M_{NA} = \begin{bmatrix} 1 & 0 \\ \frac{2a}{c} & 1 \end{bmatrix} = \begin{bmatrix} 1 & 0 \\ i \frac{4\kappa A_0^2}{c\sigma^2} & 1 \end{bmatrix}. \quad (7)$$

Now we proceed to derive the other temporal ABCD matrices representing group-velocity dispersion, SPM, bandwidth limiting, and dispersion compensation by a prism pair, respectively.

### A. Group-Velocity Dispersion

Consider that the propagation constant  $\beta(\omega)$  for coherent pulses propagating in the dispersive Ti:sapphire crystal can be approximated by the first three terms of its Taylor series expansion around center frequency  $\omega_0$  as

$$\beta(\omega) = \frac{\omega}{c} n(\omega) \approx \beta_0 + \beta'(\omega - \omega_0) + \frac{1}{2} \beta''(\omega - \omega_0)^2. \quad (8)$$

Let  $\omega' = \omega - \omega_0$ ; then

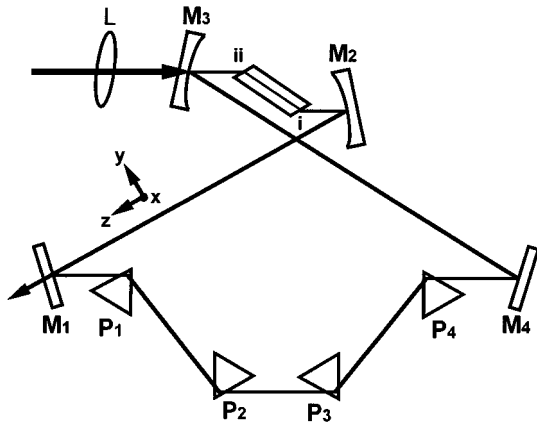


Fig. 3. Four-mirror figure-8 ring cavity laser with a Kerr medium of length  $L_c$  placed between two curved mirrors. Four Brewster-angle dispersive prisms  $P_1, P_2, P_3,$  and  $P_4$  are placed in the cavity to achieve group-velocity compensation of the laser pulses.

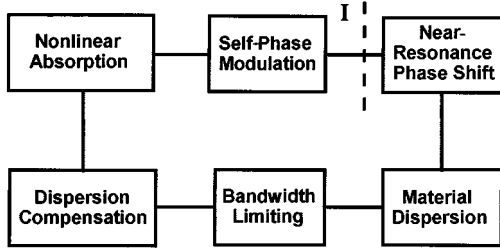


Fig. 4. Block diagram illustrating the six temporal effects in Fig. 3.

$$\frac{\omega'}{c} n(\omega') \approx \beta_0 + \frac{\omega'}{c} (n_0 + n_1 \omega'), \quad (9)$$

where  $n_0 = \beta'c$  and  $n_1 = 1/2\beta''c$ . Therefore we know from Eq. (3) that the temporal ABCD is

$$M_{DTC} = \begin{bmatrix} 1 & 2zn_1 \\ 0 & 1 \end{bmatrix} = \begin{bmatrix} 1 & \beta''cz \\ 0 & 1 \end{bmatrix}. \quad (10)$$

**B. Self-Phase Modulation**

For optical pulses passing through a thin Kerr medium the transmission coefficient (under parabolic approximation) is

$$T \approx T_0 \exp\left(i \frac{4\pi n_2 A_0^2 L_c}{\alpha_c \lambda} \frac{\tau^2}{\sigma^2}\right) = \exp(ia\tau^2), \quad (11)$$

where  $a = 4\pi n_2 A_0^2 L_c / (\alpha_c \lambda \sigma^2)$ ;  $n_2, \alpha_c,$  and  $L_c$  are the nonlinear refractive index, the correction factor, and the length of the Ti:sapphire crystal, respectively. The temporal ABCD matrix of this phase modulator is

$$M_{SPM} = \begin{bmatrix} 1 & 0 \\ \frac{2a}{c} & 1 \end{bmatrix} = \begin{bmatrix} 1 & 0 \\ \frac{8\pi n_2 A_0^2 L_c}{\alpha_c \lambda} \frac{1}{c\sigma^2} & 1 \end{bmatrix}. \quad (12)$$

However, for a thick Ti:sapphire rod, since the Gaussian beam is tightly focused in the crystal, spatial variation of

the beam spot must be taken into account. Thus  $A_0$  is not constant, and the  $A_0^2 L_c$  term in the above equation should be replaced by an integration from 0 to  $L_c$ . Therefore

$$M_{SPM} = \begin{bmatrix} 1 & 0 \\ \frac{2a}{c} & 1 \end{bmatrix} = \begin{bmatrix} 1 & 0 \\ \frac{8\pi n_2}{\alpha_c \lambda} \frac{1}{c\sigma^2} \int_0^{L_c} A_0^2 dz & 1 \end{bmatrix}. \quad (13)$$

The integration in the above equation can be related to spatial Gaussian  $q$  parameters which can be analytically calculated from Refs. 8 and 9. Let the  $q$  parameter on surface  $I$  and in the Ti:sapphire crystal be

$$\frac{1}{q_1} = \frac{1}{R_1} - i \frac{1}{y_1} = \frac{1}{R_1} - i \frac{\lambda}{n\pi w_1^2},$$

$$\frac{1}{q_2} = \frac{1}{R_2} - i \frac{1}{y_2} = \frac{1}{R_2} - i \frac{\lambda}{n\pi w_2^2},$$

respectively. Since

$$\begin{aligned} A_0^2 &= \frac{2P}{\pi w_2^2} \\ &= \frac{2nP}{\lambda y_2} \\ &= \frac{2nP}{\lambda} \frac{1}{\left(\frac{y_1}{nR_1^2} + \frac{1-K}{2y_1}\right)z^2 + \frac{2y_1}{R_1}z + ny_1}, \end{aligned} \quad (14)$$

we have

$$\begin{aligned} \int_0^{L_c} A_0^2 dz &= \frac{2nP}{\lambda} \int_0^{L_c} \frac{1}{\left(\frac{y_1}{nR_1^2} + \frac{1-K}{2y_1}\right)z^2 + \frac{2y_1}{R_1}z + ny_1} dz. \end{aligned} \quad (15)$$

The integration can be calculated easily by the following formula:

$$\int \frac{dz}{az^2 + bz + c} = \frac{2}{(4ac - b^2)^{1/2}} \tan^{-1} \frac{2az + b}{(4ac - b^2)^{1/2}}. \quad (16)$$

**C. Bandwidth Limiting**

To adjust the central wavelength of the pulses, one may insert a birefringent filter in the laser cavity; therefore the oscillation bandwidth will be limited. Even if this real filter may be absent in order to generate the shortest femtosecond pulses, other effects will still limit the pulse-width shortening, such as third- and higher-order dispersion, birefringent filtering caused by the Brewster-cut Ti:sapphire crystal, and the effect of the dispersion-compensation prism. These effects are equivalent to bandwidth limiters and must be included in our model. We approximate the spectral response of the above mechanisms by Gaussian-shaped functions.

For a Gaussian bandwidth limiter the transmission coefficient is

$$T = T_0 \exp\left(-\frac{\omega'^2}{\Delta^2}\right) \exp\left(-i \frac{\omega' n_0 z}{c}\right), \quad (17)$$

where  $\Delta$  is the half-width of the bandwidth limiter represented in angular frequency. By choosing  $n_1 = -ic/(\Delta^2 z)$ ,

$$T = T_0 \exp\left[-i \frac{\omega'(n_0 + n_1 \omega' z)}{c}\right]. \quad (18)$$

Hence we can write the temporal ABCD matrix as

$$M_{\text{BWL}} = \begin{bmatrix} 1 & 2zn_1 \\ 0 & 1 \end{bmatrix} = \begin{bmatrix} 1 & -i \frac{2c}{\Delta^2} \\ 0 & 1 \end{bmatrix}. \quad (19)$$

Comparing Eqs. (6) and (19), we found that the effect of a near-resonance phase shift is equivalent to bandwidth limiting.

#### D. Dispersion Compensation of the Prism Pair

For a single pass through the dispersion-compensation prism pair the effective negative group-velocity dispersion is<sup>12</sup>

$$\beta''z = -\frac{2\lambda^3}{\pi c^2} \left(\frac{dn}{d\lambda}\right)^2 L_p + \frac{\lambda^3}{\pi c^2} \left[\frac{d^2n}{d\lambda^2} + \left(2n - \frac{1}{n^3}\right) \left(\frac{dn}{d\lambda}\right)^2\right] d_p, \quad (20)$$

where  $L_p$  is the prism separation and  $d_p$  is the insertion width of the laser beam in the second prism  $P_2$ . The derivation of Eq. (20) is based on the marginal insertion of prisms; i.e., the cavity beam propagates through the apexes of both prisms. However, in a real system, deeper insertions are needed to reduce intracavity loss, as depicted in Fig. 5, where  $\epsilon$  is the apex angle,  $d_{p1}$  and  $d_{p2}$  are insertion width for  $P_1$  and  $P_2$ , respectively. Under such circumstances, the positive material dispersion for pulses propagating through the prisms cannot be neglected. A positive term of  $2\beta_p'' \tan(\epsilon/2)(d_{p1} + d_{p2})$ , where  $\beta_p''$  is the

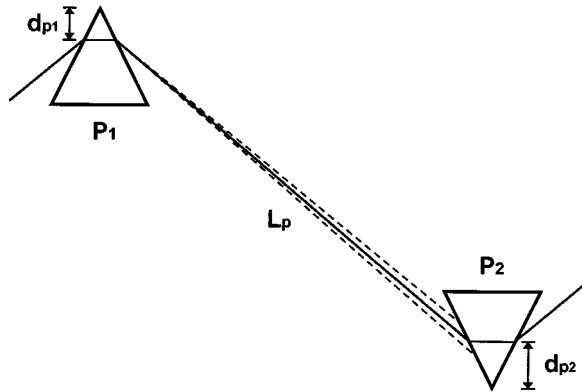


Fig. 5. In a real laser cavity, deeper prism insertions are needed to reduce intracavity loss. Here  $\epsilon$  is the apex angle, and  $d_{p1}$  and  $d_{p2}$  are the insertion widths for  $P_1$  and  $P_2$ , respectively.

material dispersion of prisms, must be included in Eq. (20). In addition,  $d_p$  can be approximated by twice the angular dispersion:<sup>12,13</sup>

$$d_p = \frac{4 \sin(\epsilon/2)}{[1 - n^2 \sin^2(\epsilon/2)]^{1/2}} \frac{dn}{d\lambda} \Delta\lambda L_p, \quad (21)$$

where  $\Delta\lambda$  is the FWHM bandwidth of the intracavity laser spectrum. Therefore the effective negative group-velocity dispersion becomes

$$\begin{aligned} \beta''z = & -\frac{2\lambda^3}{\pi c^2} \left(\frac{dn}{d\lambda}\right)^2 L_p + \frac{\lambda^3}{\pi c^2} \left[\frac{d^2n}{d\lambda^2} + \left(2n - \frac{1}{n^3}\right)\right. \\ & \times \left.\left(\frac{dn}{d\lambda}\right)^2\right] \frac{4 \sin(\epsilon/2)}{[1 - n^2 \sin^2(\epsilon/2)]^{1/2}} \frac{dn}{d\lambda} \Delta\lambda L_p \\ & + \frac{\lambda^3}{\pi c^2} \frac{d^2n}{d\lambda^2} \tan(\epsilon/2)(d_{p1} + d_{p2}). \end{aligned} \quad (22)$$

The temporal ABCD matrix for the prism pair is

$$M_{\text{DPP}} = \begin{bmatrix} 1 & 2zn_1 \\ 0 & 1 \end{bmatrix} = \begin{bmatrix} 1 & \beta''z \\ 0 & 1 \end{bmatrix}, \quad (23)$$

with  $\beta''z$  given in Eq. (22).

### 3. ANALYTICAL SPATIO-TEMPORAL FORMULATION OF KLM CAVITIES

In a previous paper<sup>9</sup> we derived a quartic equation of  $y_0 = \eta\pi\omega_0^2/\lambda$  at the output coupler for a four-mirror standing-wave cavity of Fig. 1,

$$a_4(y_0^2)^4 + a_3(y_0^2)^3 + a_2(y_0^2)^2 + a_1(y_0^2) + a_0 = 0, \quad (24)$$

where the coefficients  $a_4, a_3, a_2, a_1$ , and  $a_0$  are functions of Kerr medium length  $L_c$ , intracavity power  $P$ , and matrix elements of spatial matrices. After Eq. (24) is solved to give the beam radius at the output coupler, the beam radius within the Kerr medium can be calculated by the spatial ABCD law and renormalized  $q$  parameter propagation, and then the temporal matrix for nonlinear absorption and SPM can be calculated from Eqs. (7) and (13). In another paper<sup>10</sup> we have also analyzed the spatial behavior of the four-mirror figure-8 traveling-wave cavity in Fig. 3. The  $q$  parameters throughout the traveling-wave cavity can be calculated by solving an algebraically quadratic equation for an arbitrarily thick Kerr medium and an intracavity laser power less than self-trapping power. Again the temporal matrix for nonlinear absorption and SPM can be calculated from Eqs. (7) and (13).

Now we can proceed to find characteristic equations that describe the behavior of pulse width and chirping in the KLM cavity. As we can see from Figs. 2 and 4, the temporal effects undergone by pulses in the standing-wave and the traveling-wave cavities during a round trip differ only in their magnitude. For a traveling-wave cavity the pulses will undergo those temporal effects (except for prism-pair compensation) only once in a round trip but twice for a standing-wave cavity. Therefore in the following formulation we consider the standing-wave cavity only. The obtained results can be applied to the traveling-wave cavity after proper substitutions.

The six matrices of Fig. 2 can be lumped into two matrices:

$$\begin{bmatrix} 1 & \alpha + i\beta \\ 0 & 1 \end{bmatrix}, \quad (25)$$

$$\begin{bmatrix} 1 & 0 \\ \gamma + i\delta & 1 \end{bmatrix}. \quad (26)$$

Let the reference plane be plane  $I$ ; the round-trip temporal matrix is

$$\begin{bmatrix} A_t & B_t \\ C_t & D_t \end{bmatrix} = \begin{bmatrix} 1 + \frac{4(\alpha + i\beta)(\gamma + i\delta)}{c\sigma^2} & 2(\alpha + i\beta) \\ \frac{2(\gamma + i\delta)}{c\sigma^2} & 1 \end{bmatrix}. \quad (27)$$

The steady-state  $p$  parameter can be solved from Eq. (5) by assuming  $p_{\text{out}} = p$  owing to self-consistency. After some simple manipulation, we have

$$\frac{1}{p} = \frac{D_t - A_t}{2B_t} \pm \frac{[(D_t + A_t)^2 - 4]^{1/2}}{2B_t}. \quad (28)$$

Substituting Eqs. (2) and (27) into Eq. (28), we have

$$\frac{2\rho}{c} + i \frac{2}{c\sigma^2} = - \frac{(\gamma + i\delta)}{c\sigma^2} \pm \frac{\left[ \frac{16(\alpha + i\beta)^2(\gamma + i\delta)^2}{c^2\sigma^4} + \frac{16(\alpha + i\beta)(\gamma + i\delta)}{c\sigma^2} \right]^{1/2}}{4(\alpha + i\beta)}. \quad (29)$$

Equating the real part with the imaginary part in Eq. (29), we obtain a set of simultaneous equations of variables  $\rho$  and  $\sigma$ :

$$4\rho^2\sigma^4 + 4\gamma\rho\sigma^2 - 4(\delta + 1) = \frac{c(\alpha\gamma + \beta\delta)}{\alpha^2 + \beta^2} \sigma^2, \quad (30)$$

$$4\gamma + 4(\delta + 2)\rho\sigma^2 = \frac{c(\alpha\delta - \beta\gamma)}{\alpha^2 + \beta^2} \sigma^2. \quad (31)$$

After some tedious manipulations, a single variable equation of pulse width  $\sigma$  is derived:

$$\begin{aligned} & c^2(\alpha\delta - \beta\gamma)^2\sigma^4 + 4c(\alpha^2 + \beta^2)[\gamma\delta(\alpha\delta - \beta\gamma) \\ & - (\delta + 2)^2(\alpha\gamma + \beta\delta)]\sigma^2 - 16(\delta + 1) \\ & \times (\alpha^2 + \beta^2)^2[\gamma^2 + (\delta + 2)^2] = 0, \end{aligned} \quad (32)$$

and the chirping  $\rho$  is

$$\rho = \frac{1}{4(\delta + 2)} \left[ \frac{c(\alpha\delta - \beta\gamma)}{\alpha^2 + \beta^2} - 4 \frac{\gamma}{\sigma^2} \right]. \quad (33)$$

Since Eq. (32) is a quadratic equation of  $\sigma^2$ , the pulse width at plane  $I$  of the Kerr lens mode-locked laser system can be solved by an analytical approach. Using temporal ABCD transformation, we can calculate the pulse widths throughout the laser cavity. For example, the chirping  $\rho_1$  and the pulse width  $\sigma_1$  at output coupler are related to  $\rho$  and pulse width  $\sigma$  at plane  $I$  by

$$\rho_1 = \frac{\rho - \frac{2\alpha\rho^2}{c} - \frac{2\alpha}{c\sigma^4}}{\left( 1 - \frac{2\alpha\rho}{c} - \frac{2\beta}{c\sigma^2} \right)^2 + \left( \frac{2\alpha}{c\sigma^2} - \frac{2\beta\rho}{c} \right)^2}, \quad (34)$$

$$\sigma_1 = \frac{\left( 1 - \frac{2\alpha\rho}{c} - \frac{2\beta}{c\sigma^2} \right)^2 + \left( \frac{2\alpha}{c\sigma^2} - \frac{2\beta\rho}{c} \right)^2}{\frac{1}{\sigma^2} - \frac{2\beta\rho^2}{c} - \frac{2\beta}{c\sigma^4}}. \quad (35)$$

#### 4. KLM Ti:SAPPHIRE LASER SYSTEM DESIGN

As an example to demonstrate the applicability of the above-mentioned analytical approach, we consider a figure-x standing-wave Ti:sapphire laser, as shown in Fig. 1, with a 20-mm-long Ti:sapphire laser rod as a Kerr medium ( $n_0 = 1.76$ ,  $n_2 = 3 \times 10^{-20} \text{ m}^2 \text{ W}^{-1}$ , correction factor  $\alpha \sim 5.35$ ,  $P_{\text{cr}} \sim 2.6 \text{ MW}$ , and single-pass group-velocity dispersion of  $1280 \text{ fs}^2$ , as in Ref. 14). The distance between  $M_1$  and  $M_2$  is  $d_1 = 70 \text{ cm}$ , the distance

between  $M_3$  and  $M_4$  is  $d_2 = 100 \text{ cm}$ , and the focal length of the curved mirrors is  $f = 5 \text{ cm}$  with a separation of  $11.4 \text{ cm}$ , which is located near the center of the second stable range. The Brewster-angle dispersive prisms are made of SF10, with apex angle  $\varepsilon = 60.6^\circ$ , refractive index  $n = 1.71125$ ,  $dn/d\lambda = -0.04958 \mu\text{m}^{-1}$ , and  $d^2n/d\lambda^2 = 0.1755 \mu\text{m}^{-2}$ . As reported by several research groups, the mode-locked average power is approximately equal to that of steady-state cw. After pumping and cavity parameters (such as cavity length, mirror curvature, reflection loss of mirrors, and doping concentration of  $\text{Ti}^{3+}$ ) are specified, the cw average power can be calculated,<sup>15</sup> and the intracavity mode-locked pulse energy can be estimated accordingly. Since the Ti:sapphire laser is usually pumped far above its threshold, the spectral gain bandwidth is much larger than any other bandwidth limiter in the cavity, and thus the effect of a near-resonance phase shift can be neglected. Also, we will not consider the nonlinear gain for already saturated gain in the steady-state condition.

Now we may begin to analyze the spatio-temporal behavior of the KLM cavity. Substituting these data into the temporal ABCD matrices and using  $K = P/P_{\text{cr}}$ ,  $L_p$ , and  $\Delta\lambda$  as parameters, we solve for the output pulse width  $\sigma$  of the KLM cavity. The obtained relation between  $\sigma$  and  $K$  can further be transformed to the relation between  $\sigma$  and intracavity pulse energy  $E$ , since  $E = (\pi/2)^{1/2} \times KP_{\text{cr}}\sigma$ . In the results of the following calculations the pulse widths are given by the FWHM value  $\Delta\tau = (2 \ln 2)^{1/2}\sigma$ .

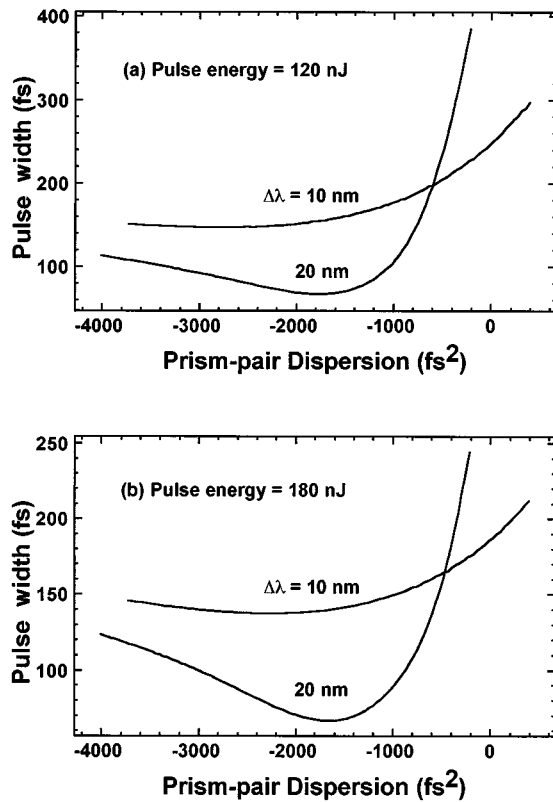


Fig. 6. Calculated FWHM pulse width at the output coupler of a standing-wave cavity for 10-nm and 20-nm intracavity bandwidths as functions of prism-pair dispersion with (a) intracavity pulse energy of 120 nJ and (b) intracavity pulse energy of 180 nJ. The distance between curved mirrors is 114 mm.

Figure 6(a) shows the dependence of output pulse widths  $\Delta\tau$  on the single-pass prism-pair dispersion for  $\Delta\lambda = 10$  nm and  $\Delta\lambda = 20$  nm, respectively. The intracavity pulse energy is 120 nJ, corresponding to 700-mW output power with 7% coupling. We found that the optimal prism separations for 10-nm and 20-nm bandwidths are different. For  $\Delta\lambda = 10$  nm, the shortest output pulses (147 fs) are obtained with  $-2780$ -fs<sup>2</sup> prism-pair dispersion, which corresponds to  $L_p = 59$  cm (the prism insertions  $d_{p1}$  and  $d_{p2}$  were chosen as 5 mm and 6 mm, respectively, for low round-trip loss), while for  $\Delta\lambda = 20$  nm the shortest output pulses (67 fs) are obtained with  $-1772$ -fs<sup>2</sup> prism-pair dispersion, which corresponds to  $L_p = 40.5$  cm (now  $d_{p1}$  and  $d_{p2}$  are chosen as 3 mm and 4 mm, because in a real system one has to minimize the

prism insertion to reduce the more severe higher-order dispersion in the sub-50-fs regime). In order to generate the shortest pulses for the KLM laser, we make the total intracavity dispersion negative. The above differences in prism separation and insertions must be taken into account in the practical KLM laser constructions. Furthermore, we notice that for broader bandwidth the pulse-width depends more strongly on the prism separation. A decrease of 20-cm separation broadens the pulse to 385 fs (5.7 times) for the 20-nm bandwidth case but only to 170 fs (1.2 times) for the 10-nm case. As a comparison, the dependence of output pulse widths on prism-pair dispersion for a pulse energy of 180 nJ is shown in Fig. 6(b). We find that the optimal prism-pair dispersion for generating the shortest pulses is reduced, which is  $-2286$  fs<sup>2</sup> for  $\Delta\lambda = 10$  nm and  $-1659$  fs<sup>2</sup> for  $\Delta\lambda = 20$  nm. The change of optimal dispersion compensation is more distinct in the narrower bandwidth case. We also notice that the shortest pulse obtainable for a 10-nm bandwidth is reduced to 137 fs, while it is almost unchanged for the 20-nm case.

Table 1 lists several published systems of a mode-locked Ti:sapphire laser<sup>4,16-19</sup> and our theoretical calculations, in which Ti:sapphire crystal lengths are equal (2 cm) and the prism materials are also SF10. Since some of these papers do not give detailed values of cavity length, intracavity power, or prism insertions, we adopt typical values. The calculated optimal prism separation and shortest pulsewidth are very close to the experimental results (within 10% and 30%, respectively), which is apparently better than the iterative numerical approach,<sup>5</sup> in which the nonlinearity is overestimated and  $n_2$  must be corrected to be 3 times less than the real value. We notice that for systems generating shorter pulses (broader bandwidth), the prism separations are also shorter, which is consistent with our theoretical prediction.

In certain circumstances we may increase the pump power to obtain higher output; then the SPM in the Ti:sapphire crystal changes as a result of increasing intracavity power. In order to realize the effect of SPM on pulse width, the dependence of  $\Delta\tau$  on pulse energy  $E$  is depicted in Figs. 7(a) and 7(b) for  $\Delta\lambda = 10$  nm and  $\Delta\lambda = 20$  nm, respectively. The pulse widths are calculated at a  $-2780$ -fs<sup>2</sup> prism-pair dispersion for a 10-nm bandwidth and a  $-1772$ -fs<sup>2</sup> dispersion for a 20-nm bandwidth. We find that as the intracavity pulse energy increases, the pulsewidth begins to decrease, which is a result of increasing SPM. However, when the pulse energy is larger than 140 nJ for a 10-nm bandwidth and 70 nJ for a 20-nm bandwidth, the pulse widths are almost unchanged.

Table 1. Prism Separation and Temporal Characteristics of Published Ti:Sapphire Laser Systems

Parameters	Gabetta <i>et al.</i> [Ref. (16)]	Pan <i>et al.</i> [Ref. (17)]	Keller <i>et al.</i> [Ref. (18)]	Cerullo <i>et al.</i> [Ref. (4)]	Rizvi <i>et al.</i> [Ref. (19)]
Prism separation (cm) experimental (theory)	80 (79)	66 (59)	41.2 (41)	35 (38)	35 (36)
Pulse width $\Delta\tau$ (fs) experimental (theory)	190 (270)	150 (145)	73 (86)	50–60 (64)	47 (54)
Bandwidth $\Delta\lambda$ (nm)	4.3	8	11.1	15	17.4
$\Delta\tau\Delta\nu$	0.39	0.58	0.33	0.36–0.43	0.39

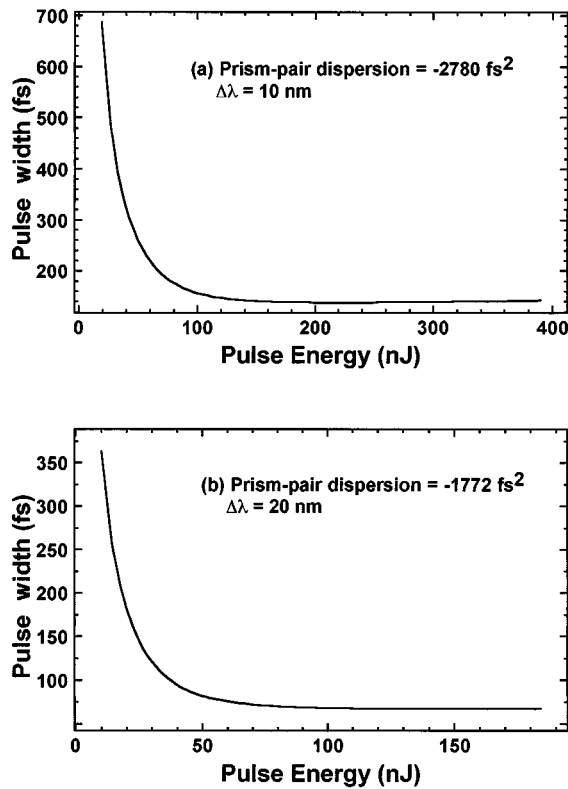


Fig. 7. Calculated pulse width at the output coupler of a standing-wave cavity as a function of intracavity pulse energy: (a) 10-nm bandwidth,  $-2780\text{-fs}^2$  prism-pair dispersion; (b) 20-nm bandwidth,  $-1772\text{-fs}^2$  prism-pair dispersion.

Next, we may compare the standing-wave cavity with the traveling-wave cavity of the same cavity length and optical components (except for an addition pair of prisms in the traveling-wave cavity). For the same output power of 700 mW the intracavity pulse energy is 240 nJ because the pulse repetition rate is only half that of the standing-wave cavity. In Fig. 8(a) we plot the output pulse widths as a function of prism separations for  $\Delta\lambda = 10$  nm. We find that the shortest pulses (95 fs) are obtained with a  $-926\text{-fs}^2$  prism-pair dispersion (corresponding to  $L_p = 27$  cm,  $d_{p1} = 3$  mm, and  $d_{p2} = 4$  mm; round-trip dispersion is  $-1852\text{ fs}^2$ ), which is quite different from the standing-wave case shown in Fig. 6(a). Since the pulses in a traveling-wave cavity propagate through the bandwidth limiter only once in a round trip, whereas for standing-wave pulses it is twice, the effective bandwidth of the traveling-wave cavity is thus  $\sqrt{2}$  times that of the standing-wave cavity, as can be seen from Eq. (19). Therefore a traveling-wave cavity is capable of producing pulses shorter than the standing-wave cavity. The dependence of  $\Delta\tau$  on pulse energy  $E$  for a traveling-wave cavity is depicted in Fig. 8(b). Again we find that the pulse width decreases as the intracavity pulse energy increases, which is the same as for a standing-wave cavity.

Finally, let us compare theoretical predictions of this analytical spatio-temporal approach with the experimental results of our self-starting KLM Ti:sapphire.<sup>20</sup> At 5-W pumping, the shortest pulses are obtained with prism separation  $L_p = 60$  cm. The prism insertions are

$d_{p1} = 5$  mm and  $d_{p2} = 6$  mm. The distance between  $M_1$  and  $M_2$  is 70 cm, and the total length between  $M_3$  and  $M_4$  is 100 cm; the distance between end face I and  $M_2$  is 49 mm, and the distance between end face II and  $M_3$  is 47 mm. The total output power (7% coupling) is 700 mW, corresponding to an intracavity pulse energy of 120 nJ. Assuming a  $\text{sech}^2$  pulse shape, the pulse width is 146 fs. From Fig. 6(a) we can see that the shortest output pulse width is 147 fs, which is obtained with a prism separation of 59 cm. Both the optimal prism separation and the shortest pulse width are very close to the experimental results, which demonstrates the accuracy of our analytical approach.

In practical systems, higher-order dispersive effects will limit the minimum achievable pulse width even though the second-order dispersion in the KLM cavity has been compensated. In fact, it was the reduction of higher-order dispersions that led to the decrease of pulse durations from  $\sim 50$  fs to the sub-10-fs regime. Since higher-order dispersion does not act as a Gaussian frequency filter, precise formulation of the pulse duration, the beam-spot size, and the KLM cavity design are beyond the scope of our analytical second-order theory. An estimation of the amount of bandwidth limited by higher order dispersions can be found in other papers.<sup>21</sup> How-

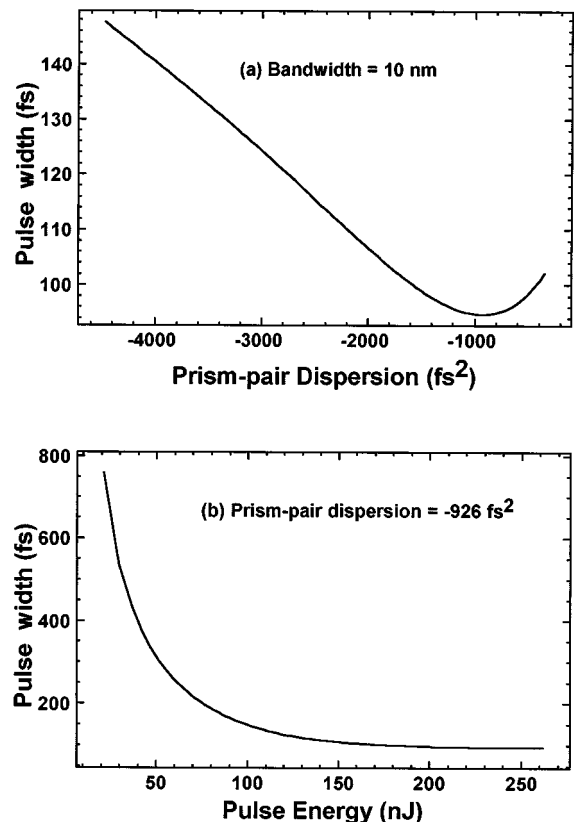


Fig. 8. (a) Output pulse width of a traveling wave cavity for a 10-nm intracavity bandwidth as a function of prism separation with intracavity pulse energy 240 nJ. The distance between curved mirrors is 112 mm. (b) Output pulse width of a traveling-wave cavity as a function of intracavity pulse energy. The bandwidth is 10 nm, and the prism-pair dispersion is  $-926\text{ fs}^2$ .

ever, analytic spatio-temporal higher order theory has, to our knowledge, not been established and is worth studying in the future.

## 5. CONCLUSIONS

In this paper we have established a general but simple spatio-temporal approach to study both the standing- and the traveling-wave Kerr lens mode-locked (KLM) laser resonators. Various spatial and temporal effects are combined to derive simple quadratic equations of pulse width for both standing- and traveling-wave cavities. By solving the quadratic equation, we obtain the relations between pulse width and other cavity parameters. We find that the optimal prism separations are shorter for broader cavity bandwidths, and the pulse width depends more strongly on the prism separation. This fact is consistent with published papers. We also find that the optimal prism separations for high-energy pulses are shorter than for low-energy pulses, which is more distinct in the narrower-bandwidth case. As the intracavity pulse energy increases, the pulse width begins to decrease, which is a result of stronger SPM and generation of more frequency components. We have explained why a traveling-wave cavity is capable of generating shorter pulses than a standing-wave cavity even if higher-order effects are not introduced. As compared with a numerical approach, the computation time of our analytic approach for cavity parameters has been reduced drastically, yet without loss of accuracy in the prediction of experimental results. Finally, we compare theoretical predictions of this analytical spatio-temporal approach with the experimental results of our self-starting KLM Ti:sapphire. Both the optimal prism separation and the shortest pulse width are very close to the experimental results, which demonstrates the accuracy of our analytical approach.

## ACKNOWLEDGMENT

The authors acknowledge partial financial support, and one of the authors, K. H. Lin, thanks the National Science Council, Taiwan, for a Ph.D. scholarship under grant NSC83-0208-M-009-066.

\*E-mail address, wfhsieh@cc.nctu.edu.tw.

## REFERENCES

1. D. E. Spence, P. N. Kean, and W. Sibbett, "60-fs pulse generation from a self-mode-locked Ti:sapphire laser," *Opt. Lett.* **16**, 42 (1991).
2. G. W. Pearson, C. Radzewicz, and J. S. Krasinski, "Analysis of self-focusing mode-locked lasers with additional highly nonlinear self-focusing elements," *Opt. Commun.* **94**, 221 (1992).
3. T. Brabec, Ch. Spielmann, P. E. Curley, and F. Krausz, "Kerr lens mode locking," *Opt. Lett.* **17**, 1292 (1992).
4. G. Cerullo, S. De Silvestri, V. Magni, and L. Pallaro, "Resonators for Kerr-lens mode-locked femtosecond Ti:sapphire lasers," *Opt. Lett.* **19**, 807 (1994).
5. J. L. A. Chilla and O. E. Martinez, "Spatial-temporal analysis of the self-mode-locked Ti:sapphire laser," *J. Opt. Soc. Am. B* **10**, 638 (1993).
6. S. P. Djaili, A. Dienes, and J. S. Smith, "ABCD matrices for dispersive pulse propagation," *IEEE J. Quantum Electron.* **26**, 1158 (1990).
7. O. O. Silichev, "Matrix method for calculations on the propagation of coherent laser pulses," *Quantum Electron.* **23**, 855 (1993).
8. L. Spinelli, B. Couillaud, N. Goldblat, and D. K. Negus, "Starting and generation of sub-100-fs pulses in Ti:Al<sub>2</sub>O<sub>3</sub> by self-focusing," in *Lasers and Electro-Optics*, Vol. 10 of 1991 OSA Technical Digest Series (Optical Society of America, Washington D.C., 1991), paper CPDP7.
9. K.-H. Lin and W.-F. Hsieh, "An analytical design of symmetrical Kerr lens mode-locking laser cavities," *J. Opt. Soc. Am. B* **11**, 737 (1994).
10. K.-H. Lin, Y. Lai, and W.-F. Hsieh, "A simple analytical method of cavity design for astigmatism compensated Kerr lens mode-locked ring lasers and its applications," *J. Opt. Soc. Am. B* **12**, 468 (1995).
11. H. A. Haus, J. G. Fujimoto, and E. P. Ippen, "Analytic theory of additive pulse and Kerr lens mode locking," *IEEE J. Quantum Electron.* **28**, 2086 (1992).
12. R. L. Fork, O. E. Martínez, and J. P. Gordon, "Negative dispersion using pairs of prisms," *Opt. Lett.* **9**, 150 (1984).
13. W. Demtröder, *Laser Spectroscopy* (Springer-Verlag, Berlin 1981), p. 128.
14. D. Huang, M. Ulman, L. H. Acioli, H. A. Haus, and J. G. Fujimoto, "Self-focusing-induced saturable loss for laser mode-locking," *Opt. Lett.* **17**, 511 (1992).
15. A. J. Alfrey, "Modeling of longitudinally pumped cw Ti:sapphire laser oscillators," *IEEE J. Quantum Electron.* **25**, 760 (1989).
16. G. Gabetta, D. Huang, J. Jacobson, M. Ramaswamy, E. P. Ippen, and J. G. Fujimoto, "Femtosecond pulse generation in Ti:Al<sub>2</sub>O<sub>3</sub> using a microdot mirror mode locker," *Opt. Lett.* **16**, 1756 (1991).
17. C.-L. Pan, C.-D. Hwang, J.-C. Kuo, J.-M. Shieh, and K.-H. Wu, "Effect of dye concentration on picosecond and femtosecond cw passively mode-locked Ti:sapphire/DDI laser," *Opt. Lett.* **17**, 1444 (1992).
18. U. Keller, G. W. 'tHooft, W. H. Knox, and J. E. Cunningham, "Femtosecond pulses from a continuously self-starting passively mode-locked Ti:sapphire laser," *Opt. Lett.* **16**, 1022 (1991).
19. N. H. Rizvi, P. M. W. French, and J. R. Taylor, "Continuously self-mode-locked Ti:sapphire laser that produces sub-50-fs pulses," *Opt. Lett.* **17**, 279 (1992).
20. J.-M. Shieh, F. Ganikhanov, K.-H. Lin, W.-F. Hsieh, and C.-L. Pan, "Completely self-starting picosecond and femtosecond Kerr-lens mode-locked Ti:sapphire laser," *J. Opt. Soc. Am. B* **12**, 945 (1995).
21. Ch. Spielmann, P. F. Curley, T. Brabec, and F. Krausz, "Ultra-broadband femtosecond lasers," *IEEE J. Quantum Electron.* **30**, 1100 (1994).